

# GPS Seismometer and its Signal Extraction

Linlin Ge

*School of Geomatic Engineering  
The University of New South Wales  
Sydney, Australia*

## BIOGRAPHY

Linlin Ge holds a B.Eng. from the Wuhan Technical University of Surveying and Mapping and a M.Sc. from the Institute of Seismology, State Seismological Bureau, P.R. China. In 1997 he was an STA Fellow, researching real-time seismology, at the Meteorological Research Institute of Japan. He is currently a Ph.D. student at the University of New South Wales, Australia, where his research interests are the interpretation of continuous GPS observations, the integration of GPS and interferometric SAR, and real-time seismology.

## ABSTRACT

The large near-field displacements before and during an earthquake are invaluable information for earthquake source study and for the detection of slow/silent quakes or pre-seismic crustal deformation events. However none of the current seismometers can measure large near-field displacements directly.

Two Leica CRS1000 GPS receivers have been used in the Real-Time Kinematic (RTK) mode with a fast sampling rate of 10Hz to test the feasibility of using a GPS receiver as a seismometer that can measure large displacements directly. Though both the 2.3Hz and 4.3Hz sine signal of 12.7mm amplitude used in the experiment to simulate seismic waves can be resolved easily from the power spectrum of the RTK time series (even for the height component), the time series itself is very noisy due to the effects of atmospheric biases, multipath, receiver noise, etc.

In order to develop an operational GPS seismometer an adaptive Finite-duration Impulse Response (FIR) filter, based on a least-mean-square (LMS) algorithm, has been designed to successfully derive a relatively noise-free seismic signal in real-time from the high-rate RTK GPS results. Several configurations of the adaptive filter are discussed.

## 1. INTRODUCTION

Typically, a seismometer (or seismograph) employs a pendulum to record seismic waves, because an "ideal pendulum" always stays in its original position regardless of the movements of the seismometer. Since the GPS satellites are not affected by earthquakes, the GPS constellation can be considered an "ideal pendulum". Therefore, a GPS receiver on Earth can be used as a seismometer if its sampling rate is high enough to recover the signature of the antenna displacement.

Accurate time synchronization for seismic networks is vital for the determination of earthquake hypocenters. Therefore, GPS has been widely used for accurate time-stamping of data collected by seismic networks. However, only recently have GPS receivers achieved very high sampling rates. State-of-the-art GPS receivers with 10 to 20Hz sampling rates are now available. This means that such new GPS receivers may be able to reproduce signals with frequencies from DC to (say) 10Hz, which is already compatible with some current seismic networks such as TERRAscope, a wide dynamic range, broad-band (10 Hz to DC) seismographic network funded by the L. K. Whittier, ARCO Foundation and NSF/ARI, USA. Hence, the concept of a "GPS seismometer" appears feasible.

Is there a need for a "GPS seismometer"? The largest amplitude of vibration accompanying an earthquake reported so far is 180mm for the 1923 Tokyo Quake and the fault displacements associated with the largest earthquakes are of the order of 30m [Turcotte, 1982]. Dr. Branson claims, "Very probably, there have been earthquakes of larger movements which our seismographs were unable to record" [Branson & Tarr, 1952]. As a matter of fact, though great efforts have been made to develop highly dynamic seismometers using the latest electronic technology, direct measurement of large co-seismic displacements with a flat frequency response remains elusive. The result is likely to be an under-estimation of earthquake sources. A GPS seismometer is therefore an option worth considering. The pendulums in a traditional seismometer are expensive fine mechanical parts. With a free "pendulum"

in space, a “GPS seismometer” is also much cheaper than a traditional one.

Two reports of experiments relating to the "GPS seismometer" concept can be found in the literature. The first experiment was carried out by the Disaster Prevention Research Institute (DPRI), Kyoto University, Japan, on 22 December 1994 [Hirahara et al., 1994]. The experiment was performed at a rover site equipped with a GPS antenna on a slider, and two reference sites at distances 160m and 160km away from this rover site. The slider oscillated horizontally with periods of 25-300sec and an amplitude of 15cm. The sampling interval of the receivers was 1sec. A horizontal accuracy of 1-2cm was achieved in post-processing and it was concluded that using GPS as a strain seismometer to obtain large amplitude near-field ground motion was possible. Another GPS seismometer experiment was carried out by the Geographical Survey Institute (GSI) of Japan, involving the kinematic processing of some of their GEONET data to derive ground motion due to the 4 October 1994, M8.1 Hokkaido-Toho-Oki earthquake [Hatanaka et al., 1994]. The sampling rate of the CGPS data was 30sec. The P-wave arrival was successfully resolved in this case. Again, the experiment suggested the feasibility of a GPS seismograph if the receiver can observe with a high enough sampling rate. Even at the 30sec sampling rate, GPS could detect slow/silent quakes or pre-seismic events.

## 2. THE UNSW GPS SEISMOMETER EXPERIMENT

At the University of New South Wales (UNSW), a GPS seismometer experiment was carried out using two Leica CRS1000 receivers. One functioned as the rover (using first a standard antenna and then a choke ring antenna), the other as the reference receiver (using a choke ring antenna only), both sampling at 10Hz and recording the raw observations. In addition, the rover was configured to record fast RTK position solutions. The experiment location was the roof of the Geography and Surveying Building (GAS) at UNSW (Fig. 1). The vibration on the GPS antenna was generated using a mechanical shaker with frequency higher than 2Hz and an amplitude of up to 12.7mm, which is more than one order improvement over previous experiments in terms of both frequency and amplitude. As shown in Fig. 2, the signal created by the sine random generator was power-amplified in order to drive the shaker. An accelerometer sensor was co-located on the GPS antenna fixture. The accelerometer output was recorded at 1200Hz by a Sony data logger.

The experiments were performed on 11 November 1998. Both standard and choke ring antennae were used. In the case of the standard antenna, the shaker was operated both vertically and when inclined to 45 degrees to the horizontal (with the antenna facing north). The shaker was vibrated at 2.3Hz, and then at 4.3Hz. Table 1 outlines how the various experimental sessions were organised.



**Figure 1. Setup of the UNSW GPS Seismometer Experiment.**

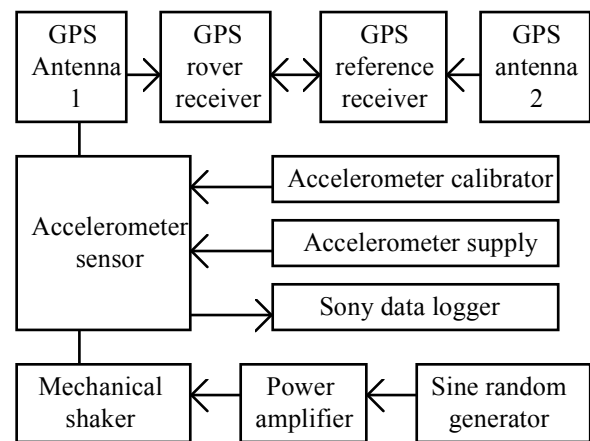


**Figure 2. System configuration for the GPS Seismometer Experiment.**

**Table 1. GPS seismometer experiment (11 November 1998).**

Time	Frequency	Antenna	Vibration
13:50	DC	Standard	Vertical
14:00	2.3Hz	Standard	Vertical
14:15	4.3Hz	Standard	Vertical
Shaker inclined 45 degree			
14:30	DC	Standard	45
14:35	2.3Hz	Standard	45
14:45	4.3Hz	Standard	45
Change to Choke Ring Antenna			
15:00	DC	Choke ring	Vertical
15:10	2.3Hz	Choke ring	Vertical
15:20	4.3Hz	Choke ring	Vertical

### 3. FAST RTK RESULTS

The recorded fast RTK results for the experiments were downloaded from the rover receiver and converted to ASCII format. A number of Matlab programs were written to process the results.

In Fig. 3, the fast RTK time series of heights for the standard antenna when stationary (upper) and vibrating (lower) can be compared. In Fig. 4, the fast RTK time series (height) when the choke ring antenna was used and vibrating at 2.3Hz (upper) and 4.3Hz (lower) are shown. In all these figures, the horizontal axis indicates the number of samples and the vertical axis the height change in meters. All signals are very noisy when viewed in the time domain, however the series are quite different if inspected closely.

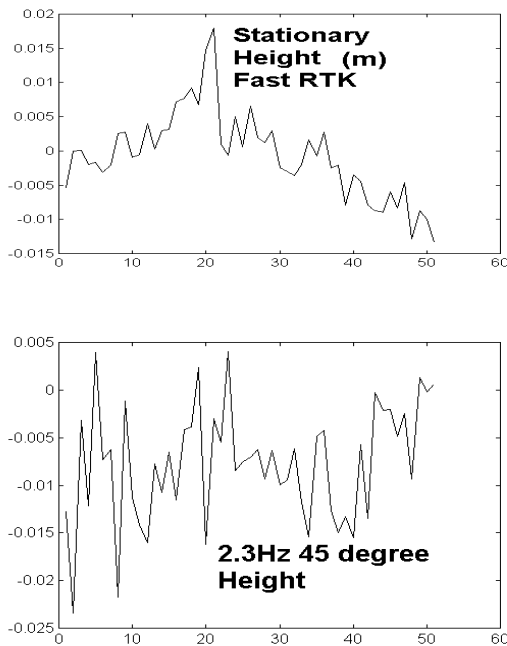


**Figure 3. Comparison of fast RTK time series when the standard antenna is stationary (upper) and vibrating (lower).**

Fig. 5 shows the frequency spectrum (after a Fast Fourier Transform (FFT) operation on the time series) comparison when the shaker was vertical but vibrated at DC (top), at 2.3Hz (middle), and at 4.3Hz (lower) respectively. The horizontal scale is in fs/2. For the UNSW experiments  $f_s=10\text{Hz}$ . All three series have the same characteristics: it is noisier in the lower band than in the higher band. Though further research on the nature of the low frequency noise is needed, major sources of GPS errors by frequency band within the range of frequencies important for seismic wave detection are [Han & Rizos, 1997; Schwarz & Wei, 1994]: (1) atmosphere: 0.00005-0.0008Hz; (2) multipath: 0.0008-0.01Hz; and (3) receiver noise: 0.0008-0.02Hz. There is also noise of an unknown source in the frequencies ranging from DC to 10 Hz.

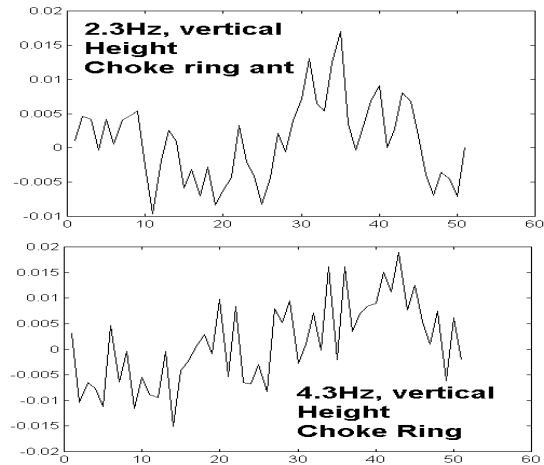


**Figure 4. Fast RTK time series using choke ring antenna.**

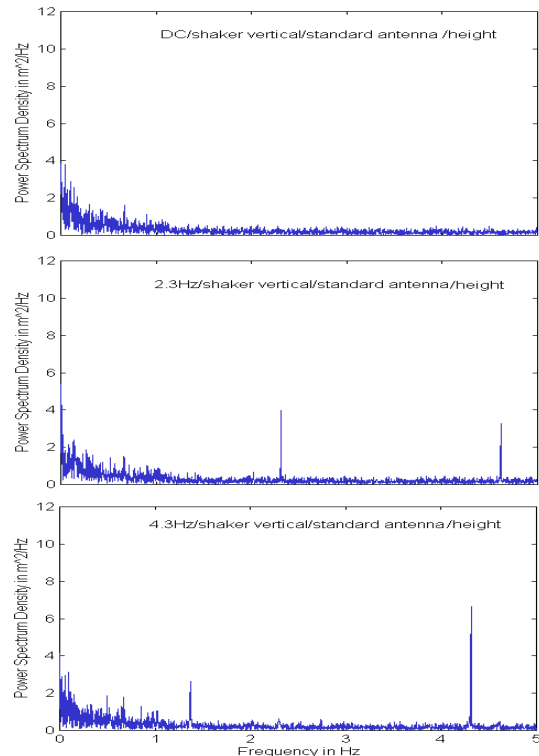


**Figure 5. Frequency spectrum comparison, shaker vertical, DC-2.3Hz-4.3Hz, standard antenna.**

The vibrations at both 2.3Hz and 4.3Hz are clearly resolved although the height in Fig. 5 is the weakest of the three components. There is also a peak at 4.6Hz in the height component when 2.3Hz was applied because the shaker could not generate a perfect sine wave. This fact had been noticed with a digital oscilloscope in the lab before the experiments and was also confirmed with the reference data from the accelerometer co-located under the GPS antenna (Fig. 6, acceleration data were resampled from 1200Hz to 64Hz when downloaded). With a 10Hz sampling rate for the GPS receiver, the 8.6Hz harmonic was removed in the case of 4.3Hz. However, the aliasing of the 8.6Hz harmonic is resolved at 1.4Hz in the lower plot of Fig. 5. It can also be seen that the 4.3Hz signal was resolved with an even better

signal-to-noise ratio (SNR) than in the case of the 2.3Hz signal.

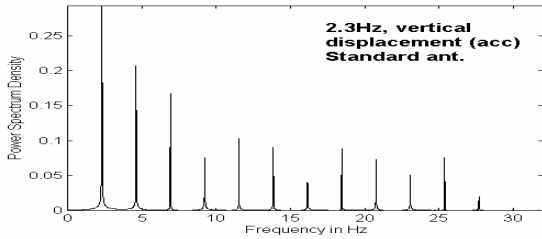


**Figure 6. Frequency spectrum from the co-located accelerometer, 2.3Hz.**

The signals, their harmonics and aliasing which can be detected with a 10Hz sampling-rate system are listed in Table 2 for the convenience of later discussions [Praokis & Manolakis, 1996].

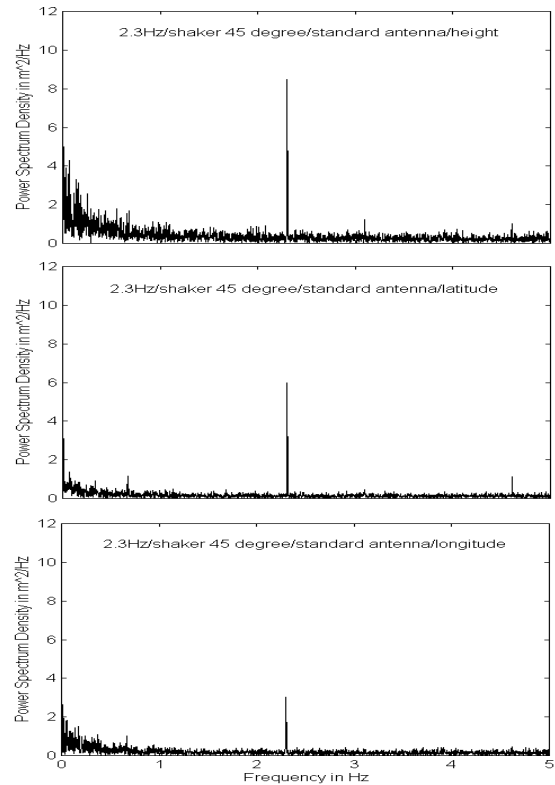
**Table 2. Signals, their harmonic and aliasing (Hz).**

signal/harmonic	aliasing	signal/harmonic	aliasing
2.3	-	4.3	-
4.6	-	8.6	1.4
6.9	3.1		
9.2	0.8		

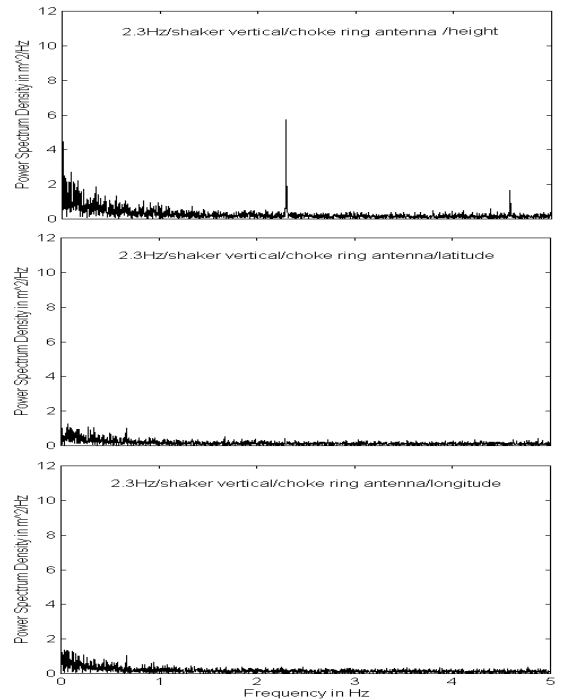
The frequency spectrum when the shaker was inclined at 45 degree (facing north) and vibrated at 2.3Hz (Fig. 7) shows that the SNR of the latitude component is higher compared to the height component, though the displacements in the two components should be roughly the same. The peak at 2.3 Hz for the longitude component indicates that the antenna was not exactly facing true north. Also the high order harmonic is seen clearly in both height and latitude components at 4.6Hz; the aliasing of the 6.9Hz harmonic in height at 3.1Hz; and the aliasing of the 9.2Hz harmonic in both latitude and longitude at 0.8Hz while it is too noisy to be seen in the height.

Fig. 8 shows the frequency spectrum when the choke ring antenna was used for the rover receiver and the shaker was vertical and vibrated at 2.3Hz, for the components of height, latitude, and longitude. The vibration at 2.3Hz is clearly resolved. There is also a peak at 4.6Hz in the height component. But there are no peaks at 2.3Hz for the latitude and longitude components, because this time a staff bubble was used to check the verticality of the shaker (which is also confirmed by a similar analysis of the data when 4.3Hz was applied). No aliasing is observed since the heavy choke ring antenna has acted as an anti-aliasing filter and greatly attenuated the harmonics. See later discussion.

Fig. 9 shows the frequency spectrum comparison when the shaker was vertical but vibrated at DC, 2.3Hz, and 4.3Hz respectively. The aliasing of the 8.6Hz harmonic can be seen in the lower plot at 1.4Hz. It can be seen that the 4.3Hz signal is resolved with an even better SNR.



**Figure 7. Frequency spectrum, 3 components, shaker 45 degree inclined, vibration 2.3Hz, standard antenna.**



**Figure 8. Frequency spectrum, 3 components, shaker vertical, vibration 2.3Hz, choke ring antenna.**

Fig. 10 shows the frequency spectrum comparison when the shaker was vertical and vibrated at 4.3Hz, for the height component, in the case of the standard antenna (upper) and the choke ring antenna (lower).

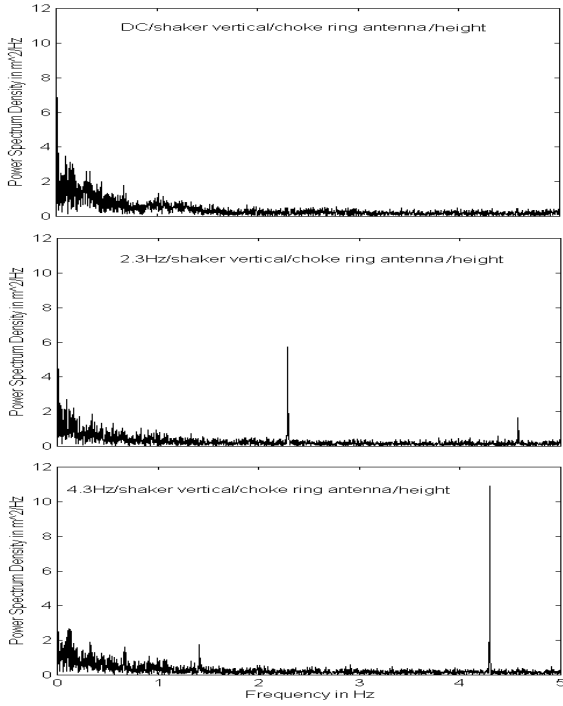


**Figure 9. Frequency spectrum for height component, shaker vertical, DC-2.3Hz-4.3Hz, choke ring antenna.**

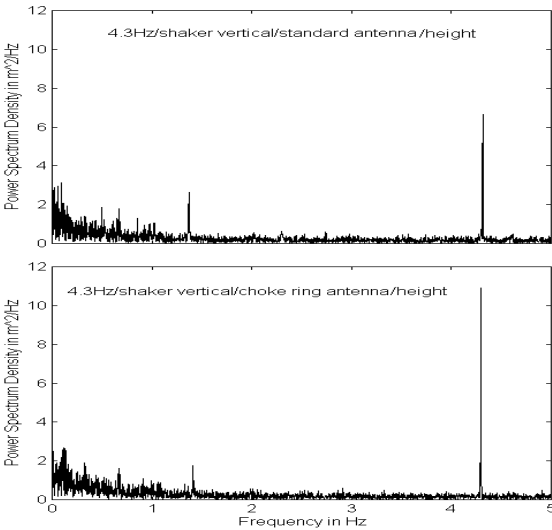


**Figure 10. Frequency spectrum for height component, comparison of 4.3Hz results for the standard and choke ring antennas.**

The noise patterns are similar for both antennae, though the magnitude of the noise is smaller for the choke ring antenna (i.e., the choke ring antenna results again indicate higher SNR). The same conclusion can be reached if the other results in Fig. 9 are compared with their equivalents in Fig. 5. The high order harmonic and aliasing are also much smaller for the results using the choke ring antenna due to the fact that it is much heavier than a standard antenna. (In fact, Prof. Randall from the School of Mechanical & Manufacturing Engineering, UNSW, has suggested that a weight be added beneath the antenna to reduce the effects of high order harmonics.)

Although from the above analysis the 2.3Hz and 4.3Hz sine waves used to simulate seismic waves can be recognized in both the time and frequency domain, they are more clearly resolved in the frequency domain. However, compared with current seismometers the results of a “GPS seismometer” is hardly acceptable even when the choke ring antenna is employed. Since the GPS noises and the broadband seismic waves fall in the same range of frequencies, and the noises are changing continuously [Han & Rizos, 1997; Lin & Rizos, 1997], the unknown filter parameters must be estimated or tuned in real-time, and changed continuously, to track and suppress the noises. Therefore, it is essential that an *adaptive* filter rather than a fixed filter be used.

As a matter of fact, applications of adaptive filters have been recognized in such diverse fields as speech analysis, seismic, acoustic, and radar signal processing, and digital filter design. In the following section, an adaptive filter based on the Least-Mean-Square algorithm is designed. The data collected from the UNSW GPS seismometer experiment are re-processed using this filter.

#### 4. ADAPTIVE FILTERING OF FAST RTK RESULTS

##### 4.1 The Adaptive Filter

An adaptive filter used for noise suppression is a dual-input, closed-loop adaptive feedback system. The operation of such an adaptive filter involves two basic processes: 1) a filtering process to produce an output in response to an input sequence, and 2) an adaptive process for the control of adjustable parameters used in the filtering process.

In the present application the dual-inputs to the adaptive filter are the primary input  $d(n)$  and the reference input  $x(n)$ , which have sample size (vector length)  $N$ , and which can be derived using several approaches as described in Section 4.5.

The primary input  $d(n)$  consists of the desired signal of interest  $s(n)$  (the seismic waves) buried in (or contaminated by) noise  $x'(n)$ , i.e.,

$$d(n) = s(n) + x'(n) \quad (1)$$

As mentioned earlier,  $x'(n)$  can be further expressed as:

$$x'(n) = x'_{atm}(n) + x'_{mul}(n) + x'_{rec}(n) + x'_{other}(n) \quad (2)$$

where  $x'_{atm}(n)$ ,  $x'_{mul}(n)$ ,  $x'_{rec}(n)$ , and  $x'_{other}(n)$  are the noise contributions from atmosphere, multipath, receiver noise, and other unknown sources, respectively.

The reference input  $x(n)$  supplies noise alone, i.e.,

$$x(n) = x_{atm}(n) + x_{mul}(n) + x_{rec}(n) + x_{other}(n) \quad (3)$$

In order to obtain a relatively noise-free signal using the adaptive filter output,  $s(n)$ ,  $x'(n)$ , and  $x(n)$  have to satisfy the following conditions:

1) the signal and noise in the primary input are uncorrelated with each other, i.e.,

$$E[s(n)x'(n-k)] = 0 \quad n, k=0, \dots, N-1 \quad (4)$$

2) the noise in the reference input is uncorrelated with the signal  $s(n)$  but is correlated with the noise component of the primary input  $x'(n)$ , i.e.,

$$E[s(n)x(n-k)] = 0 \quad n, k=0, \dots, N-1 \quad (5)$$

and

$$E[x(n)x'(n-k)] = p(k) \quad n, k=0, \dots, N-1 \quad (6)$$

where  $p(k)$  is an unknown cross-correlation for lag  $k$ .

In Section 4.5, the derivation of the primary and reference inputs for the adaptive filter which satisfies the conditions in Eq. (4), (5), and (6) is discussed. The filter must first be designed.

#### 4.2 The Filter Design

The Finite-duration Impulse Response (FIR) filter [Haykin, 1996], which is also known as a tapped delay line filter, transversal filter, all zero filter, or moving average filter, is employed in this application due to its versatility and ease of implementation.

As indicated in Fig. 11, the FIR consists of three basic elements: 1) the unit-delay elements identified by the unit-delay operator  $z^{-1}$ , where the number of elements  $M$  refers to the filter length (its order is  $M-1$ ); 2) the multipliers, whose function is to multiply the tap input by a filter coefficient (tap weight); and 3) the adders, which sum the individual multiplier outputs and yield an overall filter output:

$$y(n) = \sum_{i=0}^{M-1} \hat{w}_i(n) x(n-i) \quad (7)$$

where  $M$  is the length of the adaptive FIR filter,  $\hat{w}_i(n)$  denotes a time-varying transfer function (tap weight), which changes, or adapts, according to signal conditions, according to an algorithm which will be described in the next section.

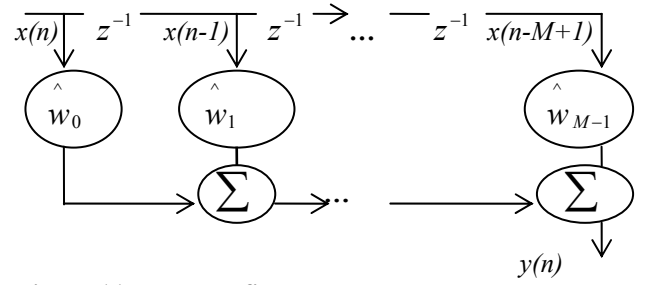


Figure 11. The FIR filter scheme.

#### 4.3 The Adaptive Algorithm Design

From Eq. (1) and (7), the estimation error:

$$e(n) = d(n) - y(n) = s(n) + x'(n) - y(n) \quad (8)$$

is used to design an algorithm for the control of the FIR filter.

Using Eq. (7) and (8), the mean square error (MSE) can be expressed as:

$$\begin{aligned} E &= \sum_{n=0}^{N-1} e^2(n) \\ &= \sum_{n=0}^{N-1} [d(n) - \sum_{i=0}^{M-1} \hat{w}_i(n) x(n-i)]^2 \\ &= \sum_{n=0}^{N-1} d^2(n) - 2 \sum_{i=0}^{M-1} \hat{w}_i(n) r_{dx}(i) \\ &\quad + \sum_{i=0}^{M-1} \sum_{l=0}^{M-1} \hat{w}_i(n) \hat{w}_l(n) r_{xx}(i-l) \end{aligned} \quad (9)$$

where

$$r_{dx}(i) = \sum_{n=0}^{N-1} d(n) x(n-i) \quad (10)$$

$$r_{xx}(i) = \sum_{n=0}^{N-1} x(n) x(n+i) \quad (11)$$

To minimize the MSE,  $E$  is partially differentiated with respect to the tap weights of the FIR filter:

$$\frac{\partial E}{\partial \hat{w}_i(n)} = 0$$

which is equivalent to:

$$\sum_{l=0}^{M-1} \hat{w}_l(n) r_{xx}(i-l) = 2r_{dx}(i), \quad i=0, \dots, M-1 \quad (12)$$

This yields the set of linear equations that generate the optimum filter coefficients at time  $n$ . To solve the equations, both the auto-correlation sequence  $\{r_{xx}(i)\}$  of the reference sequence  $\{x(n)\}$  and the

cross-correlation sequence  $\{r_{dx}(i)\}$  between the primary sequence  $\{d(n)\}$  and the reference sequence  $\{x(n)\}$  are required.

The seismic signal  $s(n)$  is indeed part of the error signal  $e(n)$  and the noise component in the adaptive filter output is  $x'(n) - y(n)$ , as indicated in Eq. (8). While  $s(n)$  is essentially unaffected by the filter, minimizing  $E$  is equivalent to minimizing the output noise  $x'(n) - y(n)$ . Therefore, the signal-to-noise ratio of the output signal is maximized.

There are two special cases when applying the adaptive filter:

- The adaptive filtering is perfect when  $y(n) = x'(n)$  and in this case the system output is noise-free, as can be seen from Eq. (8).
- The adaptive filtering will be switched off automatically, as can be seen from Eq. (12), when the reference signal  $x(n)$  is completely uncorrelated with both the signal  $s(n)$  and the noise component  $x'(n)$  of the primary signal  $d(n)$ , i.e.,  $E[d(n)x(n-k)] = 0$  for  $n, k=0, \dots, N-1$ . In this case, the primary signal is left intact and the output signal-to-noise ratio remains unchanged.

#### 4.4 The Real-time Implementation of the Adaptive Filter

As mentioned above, in order to solve the equations, both the auto-correlation sequence  $\{r_{xx}(i)\}$  of the reference sequence  $\{x(n)\}$  and the cross-correlation sequence  $\{r_{dx}(i)\}$  between the primary sequence  $\{d(n)\}$  and the reference sequence  $\{x(n)\}$  have to be calculated, which is almost impossible in real-time applications. Therefore the least-mean-square (LMS) algorithm has been introduced as an alternative computational method to adaptively adjust the coefficients (weights) of an FIR filter,  $w_i(n)$ , as in the following equation (tap-weight adaptation):

$$\hat{w}_i(n) = \hat{w}_{i-1}(n) + \mu e(n)x(n-i) \quad (13)$$

where  $\mu$  is the step size parameter,  $i = 0, \dots, M-1$  and  $n = 0, \dots, N-1$ .

It has been shown that the LMS algorithm expressed in Eq. (13) can minimize the sum of squared errors as in the case of Eq. (12) [Haykin, 1996]. Evidence has also been presented on the model-independence, and hence robust performance of the LMS algorithm [Solo & Kong, 1995], making the LMS algorithm the most widely known and used adaptive algorithm.

However, special attention has to be paid to two closely related issues: the choice of suitable value for the step-size parameter  $\mu$ , and the filter length  $M$ .

1) It is important to select an appropriate  $\mu$  which controls the rate of convergence of the LMS algorithm to the optimum solution. The larger the  $\mu$  selected, the faster the convergence. However, too large a value of  $\mu$  may result in the LMS algorithm becoming unstable. To ensure stability,  $\mu$  should be in the range [Proakis, 1995]:

$$0 < \mu < \frac{1}{10MP_x} \quad (14)$$

where  $M$  is the length of the adaptive FIR filter and  $P_x$  is the power of the reference signal, which can be approximated by:

$$P_x \approx \frac{1}{1+M} \sum_{n=0}^{N-1} x^2(n) = \frac{r_{xx}(0)}{M+1} \quad (15)$$

where  $r_{xx}(0)$  is the auto-correlation function of the reference sequence for zero lag.

2) The filter length (i.e., the number of independently adjusted parameters in the filter) should be selected so that the filter best models the regular features of a set of input data. The Minimum Description Length (MDL) criterion [Haykin, 1996] has been employed in this application. It is defined as:

$$\text{MDL}(M) = -L(\hat{\theta}_M) + \frac{1}{2} M \ln N \quad (16)$$

where  $M$  is the filter length,  $N$  is the length of the input sequence, and  $L(\hat{\theta}_M)$  is the logarithm of the maximum likelihood estimates of the filter parameters. The first term in the above equation tends to decrease rapidly with increasing  $M$  while the second term increases linearly with increasing  $M$ . Therefore there is a value of  $M$  which can minimize MDL, representing the optimum length of the filter.

In the next section, the proposed FIR filter and LMS algorithm are used to process the data from the UNSW GPS seismometer experiments.

#### 4.5 Adaptive Filtering of the GPS Seismometer Experiments

As discussed in Section 4.1, in order to obtain a relatively noise-free signal from the adaptive system, the seismic signal  $s(n)$  has to be uncorrelated with not only the RTK GPS noise  $x'(n)$  in the primary input, but also  $x(n)$  in the reference input, while  $x'(n)$  and  $x(n)$  have to be correlated with each other. To meet these conditions, three data

processing strategies have been developed, which represent three possible approaches in the implementation of a GPS seismometer.

#### 4.5.1 GPS-only Approach

This approach is illustrated in Fig. 12. Both the seismic wave  $s(n)$  and noise  $x'(n)$  are detected by the GPS receiver to generate output  $d(n)$ . The signal  $d(n)$  is delayed by  $D$  samples, i.e.,  $x(n) = d(n-D)$ , where  $D$  is chosen so that  $s(n)$  and  $s(n-D)$  are uncorrelated but  $x'(n)$  and  $x'(n-D)$  are correlated (so that  $s(n)$  and  $x(n)$  are uncorrelated but  $x'(n)$  and  $x(n)$  remain correlated). ( $s(n)$  and  $x'(n)$  are uncorrelated because they are generated from completely different physical mechanisms.)

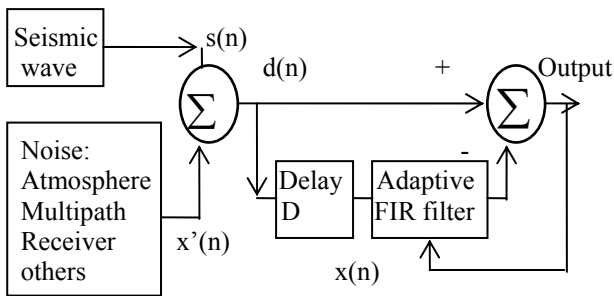


**Figure 12. Adaptive filtering configuration using the GPS-only approach.**

Fig. 13 is a sample of the result of using this approach to process the GPS seismometer experiment data with delay  $D=1$  and filter order  $M=3$  (for dataset: 2.3Hz, vertical vibration, with standard antenna).

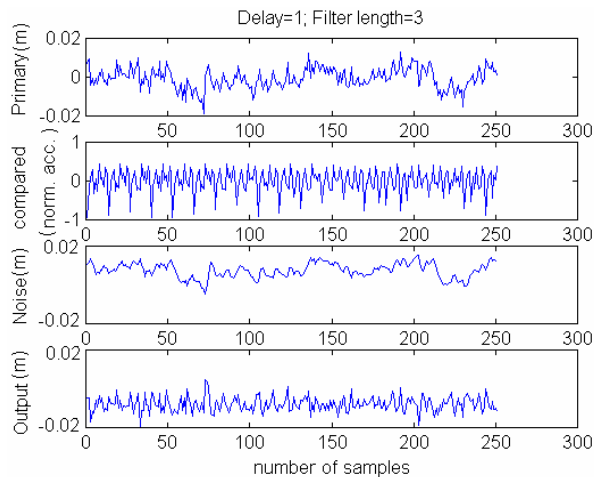


**Figure 13. Adaptive filtering result using the GPS-only approach.**

From top to bottom the plots are: the RTK GPS time sequence; accelerometer sequence for comparison only; extracted noise including atmospheric effect, multipath, receiver noise, etc.; and output from the adaptive system. In all these plots, except the second one, the horizontal axis indicates the number of samples and the vertical axis the height change in meters. In the second plot, the horizontal axis indicates the number of samples and the

vertical axis the normalized acceleration. Comparing the first and fourth plots with the second one, it can be seen that the noise has been successfully mitigated, though it has not been completely eliminated.

#### 4.5.2 GPS and Accelerometer Approach

As indicated in Fig. 14, this approach employs a two stage adaptive filter. In the first stage, the noise-corrupted seismic wave from the high sampling rate GPS receiver is used as the primary signal, while the output of the co-located accelerometer is used as the reference signal. According to Eq. (8), the output from the first stage adaptive filter is actually the noise (consisting of contributions from the atmosphere, multipath, receiver noise, etc.), which is used in the second stage as the pseudo-reference measurement. The GPS measurement is again used as primary input to the second stage adaptive filter. The adaptive algorithms used in the two stages are all LMS.

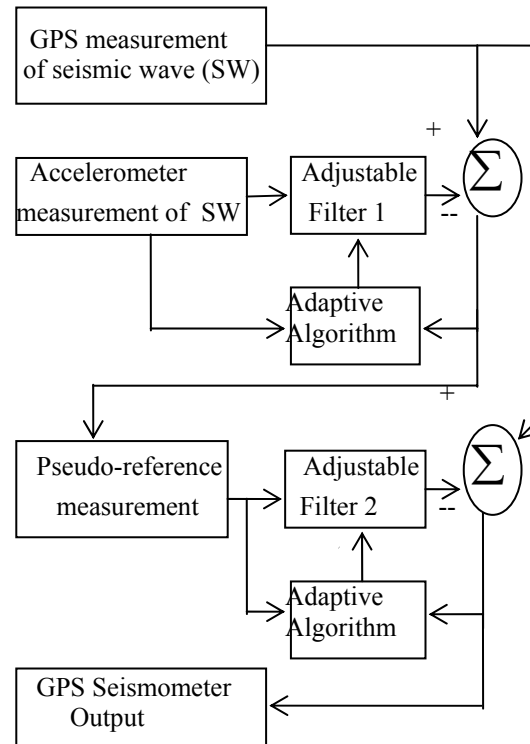


**Figure 14. Adaptive filtering configuration using the GPS and accelerometer approach.**

Fig. 15 illustrates the result of using the GPS and accelerometer approach on a sample of data. From top to bottom: the fast RTK GPS results (displacement in m); the accelerometer measurement; the noise sequence derived by the first stage filter; and the output from the second stage filter. In all these plots, except the second one, the horizontal axis indicates the number of samples and the vertical axis the height change in meters. In the second plot, the horizontal axis indicates the number of samples and the vertical axis the normalized acceleration. Comparing the first and fourth plots with the second one and with the fourth one in Fig. 13, it can be seen that

although the noise has not been removed completely, the SNR has been improved and it is now better than from the GPS-only approach.

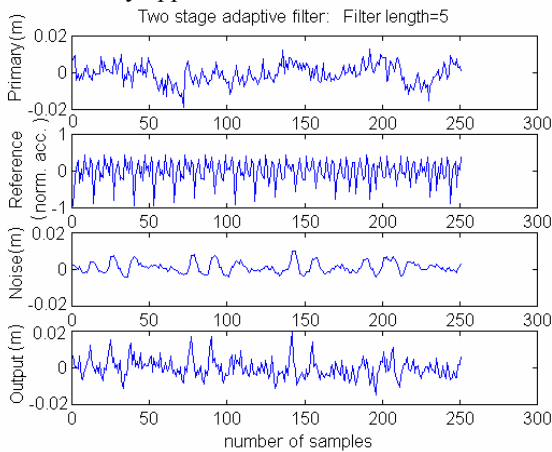


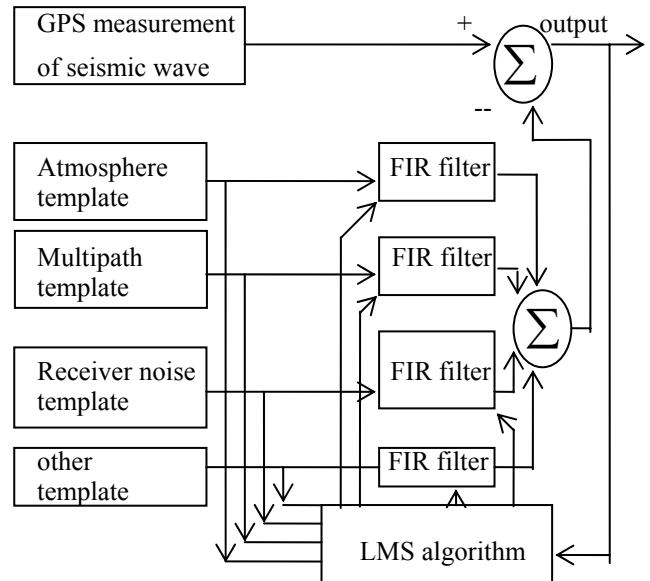
**Figure 15. Adaptive filtering result using the GPS and accelerometer approach.**

Some stations in current continuous GPS arrays such as GEONET (the Geographical Survey Institute of Japan) are already configured so that a CGPS receiver is co-located with a three-component accelerometer, which can be upgraded to a GPS seismometer using this approach. On the other hand, as mentioned earlier, GPS receivers have been widely used at many seismic stations, such as the K-NET of the National Institute for Earth Sciences and Disaster Prevention of Japan, to provide a precise time service. These stations can, therefore, be easily upgraded to output both acceleration and displacement by employing this approach.

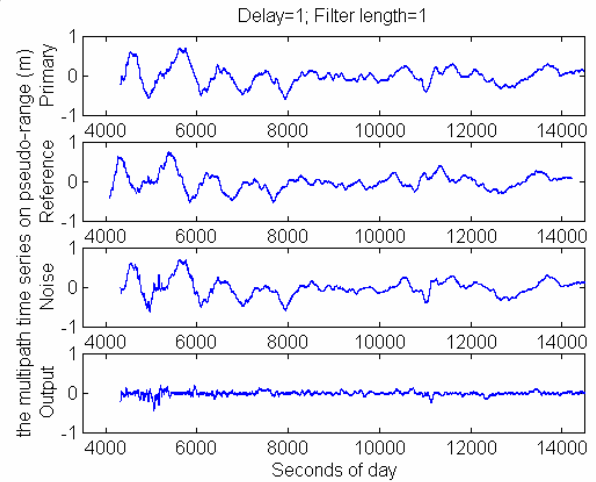
### 4.5.3 Multi-template Approach

Fig. 16 illustrates the configuration for the multi-template approach. The primary input is the GPS measurement of seismic waves represented by Eq. (1) and (2). The reference input is separated into several “templates” according to Eq. (3), which can be generated using different resources. For example, the atmospheric template can be generated using observations from adjacent GPS seismometers; the multipath template can be generated using observations on the previous day at the same site [Lin & Rizos, 1997]; and so on.

Though these resources were not available for the UNSW GPS seismometer experiments, Fig. 17 indicates adaptive filtering results using a multipath template. From top to bottom: the multipath time series of pseudo-range observations of the second day; the time series of the first day, which is used as the template; the derived noise from the adaptive filter; and the output from the adaptive filter (which shows the multipath effect has been successfully removed). The GPS data used here were the same as used in a previous study on multipath [Han & Rizos, 1997], which is actually a special case for the GPS seismometer (when there are no seismic events).



**Figure 16. Adaptive filtering configuration using the Multi-template approach.**



**Figure 17. Adaptive filtering result using the multipath-template approach.**

In another test targeting the atmospheric template, time series for 1 September 1995 and 31 October 1998 for two close stations, BRAN (latitude: 34.18489296, longitude: -118.27704570, and elevation: 246.255) and LEEP (latitude: 34.13459941, longitude: -118.32174987, and elevation: 485.062) of the Southern California Integrated GPS Network, provided by the Jet Propulsion Laboratory were used to successfully derive the tectonic movement and to generate the “template”. The results will be published in a coming paper.

This approach will be tested thoroughly with future experimental data.

## 5. CONCLUDING REMARKS

Two Leica CRS1000 GPS receivers have been used in the fast RTK mode to study the feasibility of using GPS as a broadband and highly dynamic seismometer. The sampling rates of both the rover and reference receivers were 10Hz. The rover antenna was mounted on a mechanical shaker which generates vibrations to simulate displacements due to seismic waves.

Though there was much noise in the low frequency band due to the effects of atmosphere, multipath, receiver noise, etc., FFT analysis of the fast RTK outputs indicate that vibrations of 2.3Hz and 4.3Hz with an amplitude of 12.7mm, applied to the rover antenna to simulate seismic waves, can be recognized in both the time and frequency domain (though they are more clearly resolved in the frequency domain), not only in the latitude and longitude components, but also in the height component. The fast RTK results at DC, 2.3Hz and 4.3Hz were found to exhibit similar noise patterns. The choke ring antenna is shown to yield results with higher SNR than the standard antenna. In addition to the signals, harmonics and aliasing were also detected. Data from a reference accelerometer confirmed that the harmonic was generated by the shaker and is not an artifact of the GPS experiment.

Compared with current seismometers, the output of this "GPS seismometer" is not yet acceptable even when the choke ring antenna is employed. Therefore, an adaptive filter based on the Least-Mean-Square algorithm has been designed to track and eliminate noise in real-time. Three novel approaches, namely the GPS-only, the GPS and accelerometer, and the multi-template approach, have been developed and used to process the GPS seismometer experiment data. The former two have improved the SNR of the UNSW GPS seismometer significantly, while the latter has proved to be very effective in canceling the multipath effects using data collected on a previous day. An operational GPS seismometer can therefore be developed using a high sampling rate GPS receiver and an LMS adaptive filter.

Further tests will be conducted in 1999 at UNSW as well as during field trials in Japan. The approaches developed here will also have applications in real-time seismology, GPS tsunami gauge warning systems, airborne gravimetry, and so on.

## ACKNOWLEDGEMENT

The author would like to thank his supervisors Dr. Shaowei Han and Prof. Chris Rizos for their guidance and encouragement in this research. Thanks to Dr. Yuzo Ishikawa of the Meteorological Research Institute of Japan for providing key references and contributing to discussions on the experiments. The assistance in the experiment from Prof. Randall and his PhD student Domenica from the School of Mechanical and Manufacturing Engineering, UNSW, Mr. Philip Lam, and all the members of SNAP (Satellite Navigation And

Positioning group of UNSW) is gratefully acknowledged. The CRS1000 GPS receivers were provided by Leica Geosystems.

## REFERENCES

- Branson, E. B. and W.A. Tarr, 1952. *Introduction to geology*. McGraw-Hill, New York, 3rd ed, 306pp.
- Han, S. and C. Rizos, 1997. Multipath effects on GPS in mine environments. *Xth International Congress on the International Society for Mine Surveying*, Fremantle, Australia, 2-6 November, 447-457.
- Hatanaka, Y., et al., 1994. Coseismic crustal displacements from the 1994 Hokkaido-Toho-Oki earthquake revealed by a nationwide continuous GPS array in Japan - results of GPS kinematic analysis. *Japanese Symposium on GPS (1994)*, 15-16 Dec., Tokyo, Japan, 141-147. (in Japanese)
- Haykin, S., 1996. *Adaptive filter theory*. Prentice Hall, New Jersey, 3rd ed, 989pp.
- Hirahara, K., et al., 1994. An experiment for GPS strain seismometer. *Japanese Symposium on GPS (1994)*, 15-16 Dec., Tokyo, Japan, 67-75.
- Lin, L.S. and C. Rizos, 1997. Use of multipath template technique for mitigating GPS pseudo-range multipath: methodology and test results. *First Trans Tasman Surveyors Conf.*, Newcastle, Australia, 12-18 April, paper no. 22, 1-9.
- Proakis, J.G., 1995. *Digital communications*. McGraw-Hill, New York, 3rd ed, 905pp.
- Proakis, J. G. and D. G. Manolakis 1996. *Digital signal processing: principles, algorithms, and applications*. Prentice Hall, New Jersey, 3rd ed, 968 pp.
- Schwarz, K.P. and M. Wei, 1994. Some unsolved problems in airborne gravimetry. *IAG Symposium No. 113 "Gravity and Geoid"*, Graz, Austria, 11-17 September. Springer Verlag, 131-150.
- Solo, V. and X. Kong, 1995. *Adaptive signal processing algorithms: stability and performance*. Prentice Hall, New Jersey, 1<sup>st</sup> ed, 377pp.
- Turcotte, D. L., 1982. *Geodynamics : applications of continuum physics to geological problems*. Wiley, New York, 1<sup>st</sup> ed, 450 pp.